Supplement of
Enhanced growth rate of atmospheric particles from sulfuric acid

Dominik Stolzenburg et al.

Correspondence to: Paul M. Winkler (paul.winkler@univie.ac.at)

S1 Experimental design

The CERN CLOUD chamber (detailed description can be found in Duplissy et al. (2016)) is a 26.1 m^3 stainless steel aerosol chamber, which can be kept at a constant temperature within 0.1 K precision. The dry air supply for the chamber is provided by boil-off oxygen and boil-off nitrogen mixed at the atmospheric ratio of 79:21. This ensures extremely low contaminant levels, especially from organics and sulfuric acid. Water vapour, ozone and other trace gases, such as SO_2 can be precisely added at the pptv-level. For the experiments presented here, apart from O_3 (~120 ppb), SO_2 (5 ppb), NH_3 and water (38% or 60% relative humidity), the chamber was kept clean. The cleanliness from organic contaminants was validated by the measurement of chamber air with a PTR3 proton-transfer-reaction time of flight mass spectrometer (Breitenlechner et al., 2017) and a nitrate chemical ionization-atmospheric pressure interface-time of flight mass spectrometer (nitrate CI-APi-ToF) (Jokinen et al., 2012). The absence of any contamination from amines was confirmed by measurements with a water cluster-CI-APi-ToF (Pfeifer et al., 2019), which did not register dimethylamine mixing ratios above the detection limit of 0.1 pptv. Additionally, the CLOUD experiment offers the possibility to study new particle formation under different ionization levels. Two electrode-grids one at the top and one at the bottom of the chamber can be supplied with a ±30 kV high voltage. The generated electric field clears ions and charged particles from the chamber within seconds, in order to study growth by sulfuric acid under neutral conditions. If the clearing field is switched off, ionization from galactic cosmic rays naturally increase the ion concentration inside the chamber.

The experiments were initiated by homogeneous illumination of the chamber at constant O_3 and SO_2 levels. The UV light of four Hamamatsu UV lamps guided into the chamber with fibre optics induced the photo-dissociation of O_3 and production of OH· radicals. Thereby, SO_2 is oxidized, leading to the formation of sulfuric acid. Particle growth rates were measured with the appearance time method, which requires a growing particle population, which can be clearly identified (Lehtipalo et al., 2014; Stolzenburg et al., 2018). Therefore, after the new particle population reached 10 nm, a short 30 minute cleaning stage was performed in order to increase loss rates for particles and sulfuric acid. As shown for the typical run example in Fig. S1, this leads to clearly separated growing particle populations in subsequent experiments.

30   Sulfuric acid monomer concentrations were measured with a nitrate CI-API-TOF. The sulfuric acid concentration was determined as the mean of the sum of three different molecular ion signals (HSO_4^-, $HNO_3HSO_4^-$, $(H_2O)HSO_4^-$) during the time period where the growth rate was measured. The signal is normalized by the main nitrate reagent ions and corrected for sampling line losses. Calibration of the instrument's response to sulfuric acid (Kürten et al., 2012) was performed before and after the measurement campaign and yielded comparable results.

35   Compared to previous studies, also the measurement of gas-phase NH_3 significantly improved due to the deployment of a calibrated water cluster CI-APi-ToF (Pfeifer et al., 2019). The protonated water cluster reagent ions selectively ionize ammonia and amines at ambient pressure. The detection limits reach approximately 0.5 pptv for ammonia and 0.1 pptv for dimethylamine. The data measured by the water cluster CI-APi-ToF were cross-checked at high NH_3 concentrations against a commercial PICARRO NH_3 analyser.

40

     Particle growth was monitored using a DMA-train (Stolzenburg et al., 2017) for the size-range of 1.8-8 nm and a TSI Model 3936 nano-SMPS for sizes larger than 5 nm. Both instruments use electrical mobility classification in order to infer a particle size-distribution. Compared to the scanning particle-size-magnifier (see e.g. Lehtipalo et al., 2014), which was used as the main instrument for particle growth measurements in Lehtipalo et al. (2016), these instruments have less systematic

45 uncertainties on the actual size classification. The size-ranges of both studies are therefore not directly comparable. We show the measurements in the lower size-interval of the DMA-train (1.8-3.2 nm) together with the earlier results (size range 1.5-2.5 nm) in Fig. S2. The results with ammonia added to the chamber, which presumably decreases the evaporation rates to close to zero, agree nicely with the collision enhanced kinetic limit of this study, when the size-range is adjusted. Particle growth rates are inferred with the appearance time method (Lehtipalo et al., 2014; Stolzenburg et al., 2018). Figure S1d demonstrates for a

50 representative experiment how the signal in each size channel of the used mobility analysers is fitted by a sigmoidal shape curve in order to infer the 50 % appearance time, i.e. the time where 50 % of the maximum signal intensity during the run is reached first. The appearance times are plotted versus the corresponding diameter and fitted with a linear function over the two size intervals 1.8-3.2 nm and 3.2-8 nm. Nanoparticle growth rates inferred via this method could be affected by a strong contribution of cluster coagulation (Kontkanen et al., 2016; Li and McMurry, 2018). However, the comparison with a

55 modelling study in Fig. S3 indicates that this contribution is expected to be negligible. Moreover we also used the size- and time-resolving growth rate analysis method INSIDE (Pichelstorfer et al., 2018) which accounts for coagulation and wall losses to cross-check our results (Fig. 4b).

S2 Theory of growth caused by sulfuric acid condensation

     Our description of particle growth rates follows the approach of Nieminen et al., (2010), but with a modified kinetic coefficient

60 (Chan and Mozurkewich, 2001). Accordingly, the particle growth rate (GR) is defined as:

$$GR = \frac{\mathrm{d}d_p}{\mathrm{d}t} = \frac{\frac{\mathrm{d}V_p}{\mathrm{d}t}}{\frac{\mathrm{d}V_p}{\mathrm{d}d_p}} = \frac{2 \cdot k_{coll} \cdot V_v \cdot C_v}{\frac{\mathrm{d}}{\mathrm{d}d_p}[\frac{\pi}{6}d_p^3]}, \tag{S1}$$

where d_p is the growing particle diameter, V_p and V_v are the volume of particle and vapor molecule, C_v is the vapor monomer concentration and k_{coll} is the kinetic collision frequency between particle and vapor, which is accounted for twice to include collisions in both ways. The accommodation coefficient is assumed to be unity. We use a collision frequency which allows for a collision enhancement of neutral vapours and particles due to attractive London-van-der-Waals forces (Chan and Mozurkewich, 2001):

$$k_{coll}(d_v, d_p) = k_K \cdot \left(\sqrt{1 + \left(\frac{k_K}{k_D}\right)^2} - \left(\frac{k_K}{k_D}\right) \right), \tag{S2}$$

with $k_K = \frac{\pi}{8} \cdot (d_v + d_p)^2 \cdot \left(\frac{8kT}{\pi}\right)^{1/2} \cdot \left(\frac{1}{m_v} + \frac{1}{m_p}\right)^{1/2} \cdot E(\infty)$ and $k_D = 2\pi \cdot (d_v + d_p) \cdot (D_v + D_p) \cdot E(0)$ as the kinetic collision rates for the free molecule and continuum regime, respectively. They depend on the diameters $d_{v/p}$ the masses $m_{v/p}$ and the diffusion coefficients $D_{v/p}$ of the colliding vapor molecules or particles, respectively. However, compared to Nieminen et al. (2010), but include collision enhancement factors due to London-van-der-Waals forces, $E(\infty)$ and $E(0)$, which can be linked to the reduced Hamaker constant A' with the parameters a_n and b_m (Chan and Mozurkewich, 2001):

$$E(\infty) = 1 + \frac{\sqrt{A'/3}}{1 + b_0\sqrt{A'}} + b_1 \cdot \ln(1 + A') + b_2 \cdot \ln^3(1 + A'), \tag{S3}$$

$$E(0) = 1 + a_1 \cdot \ln(1 + A') + a_2 \cdot \ln^3(1 + A'), \tag{S4}$$

The reduced Hamaker constant relates to the Hamaker constant A, which describes the potential of van-der-Waals forces between two spherical particles (Hamaker, 1937):

$$A' = \frac{A}{kT} \frac{4d_v d_p}{(d_v + d_p)^2}, \tag{S5}$$

In this study we use this updated condensation equation Eq. (S1) and integrate it numerically over the size interval used for the determination of the growth rate $[d_{\mathrm{init}}, d_{\mathrm{final}}]$:

$$GR\,(d_{\mathrm{init}}, d_{\mathrm{final}}) = \frac{\Delta d_p}{\Delta t} = (d_{\mathrm{final}} - d_{\mathrm{init}}) \Big/ \int_{d_{\mathrm{init}}}^{d_{final}} \frac{\pi/2 \cdot d_p^2}{2 \cdot k_{coll} \cdot V_v \cdot C_v}\,\mathrm{d}d_p, \tag{S6}$$

S2.1 Assumed properties of the condensing clusters and systematic uncertainties

Eq. (S6) includes several properties of the condensing vapour. The volume of a monomer can be linked to its molecular mass and density $V_V = m_v/\rho_v$. However, sulfuric acid molecules might co-condense with water, as gas-phase sulfuric acid is usually hydrated at typical ambient relative humidity (Hanson and Eisele, 2000; Kurtén et al., 2007). The density of the condensing cluster is described by the macroscopic density of sulfuric acid water solutions (Myhre et al., 1998):

$$\rho_{v/p}(w, T)[\mathrm{kg\,m^{-3}}] = \sum_{i=0}^{10} \sum_{j=0}^{4} \rho_{i,j} w^i \cdot (T[\mathrm{K}] - 273.15)^j, \tag{S7}$$

where w is the mass fraction of sulfuric acid in solution with $(1 - w)$ water. The coefficients ρ_{ij} can be found in Myhre *et al.* (Myhre et al., 1998). The mass fraction is inferred from the assumed molecular composition of the nucleating clusters. Therefore, we will also use the mass fraction of $w = 98./m_v$ depending on the vapor molecular mass.

90   The molecular mass of the condensing sulfuric acid water clusters is not directly measured, as e.g. water might evaporate inside the nitrate CI-APi-ToF. Any gas-phase sulfuric acid will always exist in a mixture of different hydrated states. Quantum chemical simulations indicate that the effect of relative humidity on sulfuric acid vapour monomer hydration favours 2 water molecules attached to the sulfuric acid core molecule at 50% relative humidity (which is chosen to represent our measurements at 60% and 38% relative humidity) (Kurtén et al., 2007). This will result in a vapour molecular mass of $m_v = 134$ amu. In the

95   presence of ammonia, nucleation of this ternary system proceeds with sulfuric acid in excess of ammonia (Hanson and Eisele, 2002): only one ammonia molecule is needed to stabilize a sulfuric acid dimer efficiently, which we also assume to hold true for larger particle sizes. If per two condensing sulfuric acid molecules, one ammonia molecule is bound to the particle, the mass per condensing cluster is increased by $m_{NH3}/2 = 8.5$ amu, and hence $m_v = 142.5$ amu for all growth measurements where ammonia was added to the chamber.

100   The last property of the condensing vapour for the computation of Eq. (S6) is the diffusion coefficient of sulfuric acid. As also the diffusion coefficient depends on the degree of hydration of the sulfuric acid molecule, we use relative humidity dependence of the diffusion coefficient for sulfuric acid as follows (Hanson and Eisele, 2000):

$$D_v(RH[\%]) = \frac{1}{p[\text{atm}]} \cdot \left(\frac{T[K]}{298}\right)^{1.75} \cdot \frac{p_0 D_0 + p_0 D_1 \cdot K_1 \cdot RH + p_0 D_2 \cdot K_1 K_2 \cdot (RH)^2}{1 + K_1 RH + K_1 K_2 (RH)^2}, \tag{S8}$$

which includes corrections for pressure and temperature different to the original experimental values. The fitting constants

105   and the values for the diffusivity of the pure monomer, the singly hydrated monomer and the doubly hydrated monomer ($p_0 D_0$, $p_0 D_1$, $p_0 D_2$, respectively) can be found in Hanson and Eisele (2000). The diffusivity of the growing particles can be described using their measured mobility diameter and Stoke's law, including the dynamic viscosity of air η and the Cunningham slip correction factor $C(d_p)$:

$$D_p = \frac{kT \, C(d_p)}{3\pi\eta d_p}, \tag{S9}$$

110   Main systematic uncertainties in the estimate of the Hamaker constant might be related to the assumed properties of the condensing clusters. In order to explore the wide range of systematic uncertainties, we ran the fitting algorithm 10000 times, randomly assigning different parameters, summarized in Fig. S3. We use with equal probabilities either the pure sulfuric acid water solution density at the specified temperature (S7), or a combined sulfuric acid, water and ammonia density at 298 K (Hyvärinen et al., 2005). Also with equal probabilities we use two different approaches for the diffusion coefficient of the

115   vapour, either Eq. (S8) or the approach of Cox and Chapman (2001). With an equal probability we either use 1, 2 or 3 water molecules as assumed degree of hydration. Independent of the assumed properties of the condensing cluster is the systematic uncertainty of the sulfuric acid concentrations, which is estimated by assigning a multiplicative offset to all sulfuric acid measurements, which follows a lognormal distribution with median 1 and shape parameter $\sigma_g = 0.5/3$, assuring that with

99.7% probability the resulting systematic sulfuric acid offset is within the interval of +50/-33 %, which represents the
systematic uncertainty in the absolute sulfuric acid calibration (Kürten et al., 2012). Fig. S3 shows that the systematic
uncertainty of the nitrate CI-APi-ToF measurement of H_2SO_4 is by far the largest source of uncertainty in our Hamaker constant
estimate compared to the different approaches for the diffusivity and density of the condensing cluster.

S3 Global model

We implement the results of our growth-rate measurements for sulfuric acid driven growth in a global model (Mann et al.,
2010; Mulcahy et al., 2018), which includes sulfuric acid-water binary nucleation. As we do not observe any significant effect
of ammonia on growth for particles larger than the nucleation size in the model (1.7 nm), we used the same implementation
for growth caused by sulfuric acid for the entire model. However, the model does not include ternary nucleation schemes
(Dunne et al., 2016) and pure biogenic nucleation (Gordon et al., 2016) and will therefore underestimate the impact of
nucleation on the global aerosol and CCN budget. In the model, growth between the nucleation size and 3 nm is treated with
the equation of Kerminen and Kulmala (Kerminen and Kulmala, 2002), which gives the fraction of particles surviving to 3 nm
at a given growth rate and loss rate. Here as a baseline case we use the geometric hard-sphere kinetic growth rate based on
bulk-density (Nieminen et al., 2010) and compare this to the collision enhanced growth, which is a factor of 2.2 higher over
the size-interval between the nucleation size and 3 nm. For larger sizes, aerosol growth in the model is calculated by solving
the condensation equations. Therefore no direct growth parametrization can be altered, but as condensational growth scales
linearly with the diffusion coefficient of the condensing vapour, we increased sulfuric acid diffusion by a factor of 1.8 for
condensation in the nucleation mode (2-10 nm) and 1.3 for condensation in the Aitken mode (10-100 nm). The enhancement
factors are derived according to Fig. 4a for the median diameters of the modes (7.6 and 57 nm respectively) at cloud base level
(1 km). However, this constant factor of increase in diffusion coefficient, and hence flux onto particles, for all particles of the
entire mode, might underestimate the impact of the collision enhancement. Rapid growth is increasingly important for the
smallest particles, which actually have a higher collision enhancement compared to particles with the size of the mode median
diameters.

Supplementary References

Breitenlechner, M., Fischer, L., Hainer, M., Heinritzi, M., Curtius, J. and Hansel, A.: PTR3: An Instrument for Studying the
Lifecycle of Reactive Organic Carbon in the Atmosphere, Anal. Chem., 89(11), 5824–5831,
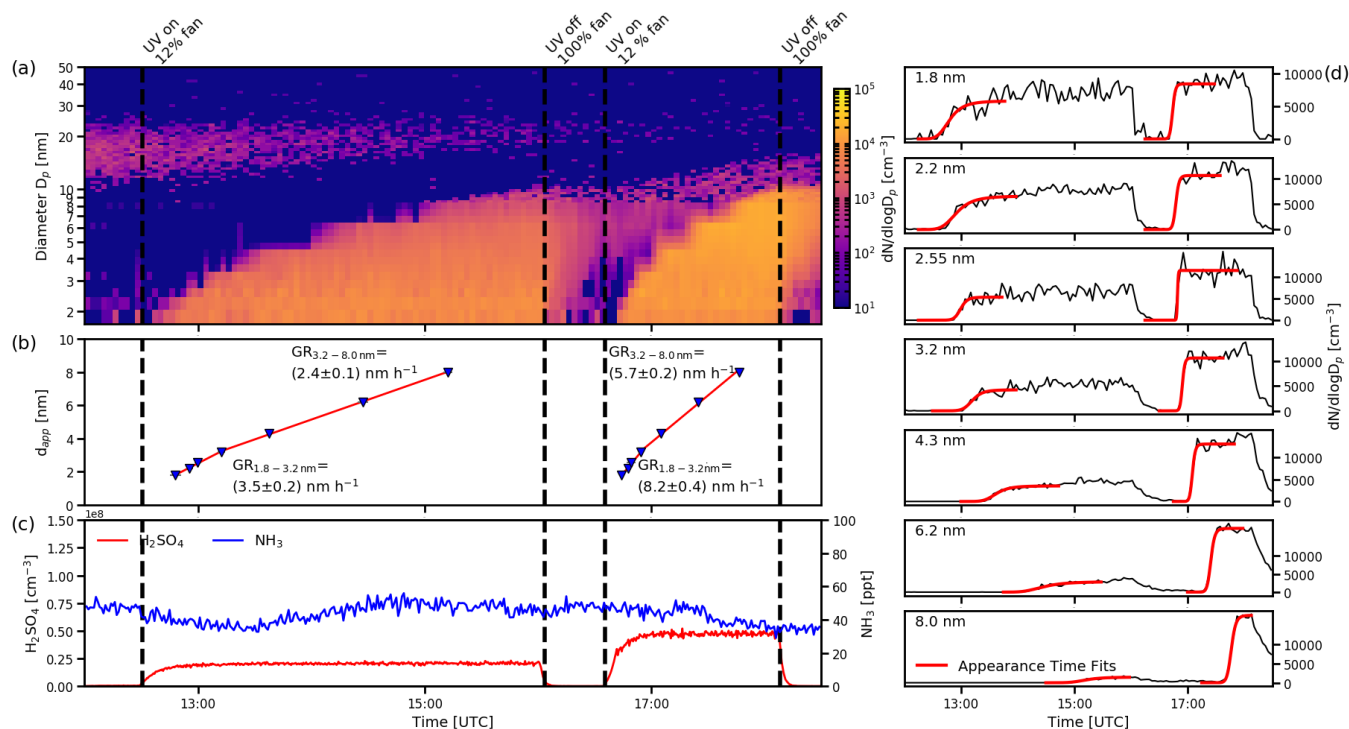doi:10.1021/acs.analchem.6b05110, 2017.

Chan, T. W. and Mozurkewich, M.: Measurement of the coagulation rate constant for sulfuric acid particles as a function of
particle size using tandem differential mobility analysis, J. Aerosol Sci., 32(3), 321–339, doi:http://dx.doi.org/10.1016/S0021-
8502(00)00081-1, 2001.

Cox, K. R. and Chapman, W. G.: The Properties of Gases and Liquids, 5th ed., edited by B. E. Poling, J. M. Prausnitz, and J. P. O'Connell, McGraw-Hill, New York., 2001.

Dunne, E. M., Gordon, H., Kürten, A., Almeida, J., Duplissy, J., Williamson, C., Ortega, I. K., Pringle, K. J., Adamov, A., Baltensperger, U., Barmet, P., Benduhn, F., Bianchi, F., Breitenlechner, M., Clarke, A., Curtius, J., Dommen, J., Donahue, N. M., Ehrhart, S., Flagan, R. C., Franchin, A., Guida, R., Hakala, J., Hansel, A., Heinritzi, M., Jokinen, T., Kangasluoma, J., Kirkby, J., Kulmala, M., Kupc, A., Lawler, M. J., Lehtipalo, K., Makhmutov, V., Mann, G., Mathot, S., Merikanto, J., Miettinen, P., Nenes, A., Onnela, A., Rap, A., Reddington, C. L. S., Riccobono, F., Richards, N. A. D., Rissanen, M. P., Rondo, L., Sarnela, N., Schobesberger, S., Sengupta, K., Simon, M., Sipilä, M., Smith, J. N., Stozhkov, Y., Tomé, A., Tröstl, J., Wagner, P. E., Wimmer, D., Winkler, P. M., Worsnop, D. R. and Carslaw, K. S.: Global atmospheric particle formation from CERN CLOUD measurements, Science (80-.)., 354(6316), 1119–1124, doi:10.1126/science.aaf2649, 2016.

Duplissy, J., Merikanto, J., Franchin, A., Tsagkogeorgas, G., Kangasluoma, J., Wimmer, D., Vuollekoski, H., Schobesberger, S., Lehtipalo, K., Flagan, R. C., Brus, D., Donahue, N. M., Vehkamäki, H., Almeida, J., Amorim, A., Barmet, P., Bianchi, F., Breitenlechner, M., Dunne, E. M., Guida, R., Henschel, H., Junninen, H., Kirkby, J., Kürten, A., Kupc, A., Määttänen, A., Makhmutov, V., Mathot, S., Nieminen, T., Onnela, A., Praplan, A. P., Riccobono, F., Rondo, L., Steiner, G., Tome, A., Walther, H., Baltensperger, U., Carslaw, K. S., Dommen, J., Hansel, A., Petäjä, T., Sipilä, M., Stratmann, F., Vrtala, A., Wagner, P. E., Worsnop, D. R., Curtius, J. and Kulmala, M.: Effect of ions on sulfuric acid-water binary particle formation: 2. Experimental data and comparison with QC-normalized classical nucleation theory, J. Geophys. Res.-Atmos., 121(4), 1752–1775, doi:10.1002/2015JD023539, 2016.

Gordon, H., Sengupta, K., Rap, A., Duplissy, J., Frege, C., Williamson, C., Heinritzi, M., Simon, M., Yan, C., Almeida, J., Tröstl, J., Nieminen, T., Ortega, I. K., Wagner, R., Dunne, E. M., Adamov, A., Amorim, A., Bernhammer, A.-K., Bianchi, F., Breitenlechner, M., Brilke, S., Chen, X., Craven, J. S., Dias, A., Ehrhart, S., Fischer, L., Flagan, R. C., Franchin, A., Fuchs, C., Guida, R., Hakala, J., Hoyle, C. R., Jokinen, T., Junninen, H., Kangasluoma, J., Kim, J., Kirkby, J., Krapf, M., Kürten, A., Laaksonen, A., Lehtipalo, K., Makhmutov, V., Mathot, S., Molteni, U., Monks, S. A., Onnela, A., Peräkylä, O., Piel, F., Petäjä, T., Praplan, A. P., Pringle, K. J., Richards, N. A. D., Rissanen, M. P., Rondo, L., Sarnela, N., Schobesberger, S., Scott, C. E., Seinfeld, J. H., Sharma, S., Sipilä, M., Steiner, G., Stozhkov, Y., Stratmann, F., Tomé, A., Virtanen, A., Vogel, A. L., Wagner, A. C., Wagner, P. E., Weingartner, E., Wimmer, D., Winkler, P. M., Ye, P., Zhang, X., Hansel, A., Dommen, J., Donahue, N. M., Worsnop, D. R., Baltensperger, U., Kulmala, M., Curtius, J. and Carslaw, K. S.: Reduced anthropogenic aerosol radiative forcing caused by biogenic new particle formation, P. Nat. Acad. Sci. USA, 113(43), 12053–12058, doi:10.1073/pnas.1602360113, 2016.

Hamaker, H. C.: The London—van der Waals attraction between spherical particles, Physica, 4(10), 1058–1072, doi:https://doi.org/10.1016/S0031-8914(37)80203-7, 1937.

180   Hanson, D. R. and Eisele, F.: Diffusion of H2SO4 in Humidified Nitrogen: Hydrated H2SO4, J. Phys. Chem. A, 104(8), 1715–1719, doi:10.1021/jp993622j, 2000.

Hanson, D. R. and Eisele, F. L.: Measurement of prenucleation molecular clusters in the NH3, H2SO4, H2O system, J. Geophys. Res. Atmos., 107(D12), 10–18, doi:10.1029/2001JD001100, 2002.

Hyvärinen, A.-P., Raatikainen, T., Laaksonen, A., Viisanen, Y. and Lihavainen, H.: Surface tensions and densities of H$_2$SO$_4$ + NH$_3$ + water solutions, Geophys. Res. Lett., 32(16), L16806, doi:10.1029/2005GL023268, 2005.

Jokinen, T., Sipilä, M., Junninen, H., Ehn, M., Lönn, G., Hakala, J., Petäjä, T., Mauldin III, R. L., Kulmala, M. and Worsnop, D. R.: Atmospheric sulphuric acid and neutral cluster measurements using CI-APi-TOF, Atmos. Chem. Phys., 12(9), 4117–4125, doi:10.5194/acp-12-4117-2012, 2012.

Kerminen, V.-M. and Kulmala, M.: Analytical formulae connecting the "real" and the "apparent" nucleation rate and the nuclei number concentration for atmospheric nucleation events, J. Aerosol Sci., 33(4), 609–622, doi:10.1016/S0021-8502(01)00194-X, 2002.

Kontkanen, J., Olenius, T., Lehtipalo, K., Vehkamäki, H., Kulmala, M. and Lehtinen, K. E. J.: Growth of atmospheric clusters involving cluster-cluster collisions: comparison of different growth rate methods, Atmos. Chem. Phys., 16(9), 5545–5560, doi:10.5194/acp-16-5545-2016, 2016.

195   Kürten, A.: New particle formation from sulfuric acid and ammonia: nucleation and growth model based on thermodynamics derived from CLOUD measurements for a wide range of conditions, Atmos. Chem. Phys., 19(7), 5033–5050, doi:10.5194/acp-19-5033-2019, 2019.

Kürten, A., Rondo, L., Ehrhart, S. and Curtius, J.: Calibration of a Chemical Ionization Mass Spectrometer for the Measurement of Gaseous Sulfuric Acid, J. Phys. Chem. A, 116(24), 6375–6386, doi:10.1021/jp212123n, 2012.

200   Kurtén, T., Noppel, M., Vehkamäki, H., Salonen, M. and Kulmala, M.: Quantum chemical studies of hydrate formation of H2so 4 and HSO4-, Boreal Environ. Res., 12(3), 431–453, 2007.

Lehtipalo, K., Leppä, J., Kontkanen, J., Kangasluoma, J., Franchin, A., Wimmer, D., Schobesberger, S., Junninen, H., Petäjä, T., Sipilä, M., Mikkilä, J., Vanhanen, J., Worsnop, D. R. and Kulmala, M.: Methods for determining particle size distribution and growth rates between 1 and 3 nm using the Particle Size Magnifier, Boreal Environ. Res., 19(suppl. B), 215–236, 2014.

205   Lehtipalo, K., Rondo, L., Kontkanen, J., Schobesberger, S., Jokinen, T., Sarnela, N., Kürten, A., Ehrhart, S., Franchin, A., Nieminen, T., Riccobono, F., Sipilä, M., Yli-Juuti, T., Duplissy, J., Adamov, A., Ahlm, L., Almeida, J., Amorim, A., Bianchi, F., Breitenlechner, M., Dommen, J., Downard, A. J., Dunne, E. M., Flagan, R. C., Guida, R., Hakala, J., Hansel, A., Jud, W., Kangasluoma, J., Kerminen, V.-M., Keskinen, H., Kim, J., Kirkby, J., Kupc, A., Kupiainen-Määttä, O., Laaksonen, A., Lawler,

M. J., Leiminger, M., Mathot, S., Olenius, T., Ortega, I. K., Onnela, A., Petäjä, T., Praplan, A., Rissanen, M. P., Ruuskanen, T., Santos, F. D., Schallhart, S., Schnitzhofer, R., Simon, M., Smith, J. N., Tröstl, J., Tsagkogeorgas, G., Tomé, A., Vaattovaara, P., Vehkamäki, H., Vrtala, A. E., Wagner, P. E., Williamson, C., Wimmer, D., Winkler, P. M., Virtanen, A., Donahue, N. M., Carslaw, K. S., Baltensperger, U., Riipinen, I., Curtius, J., Worsnop, D. R. and Kulmala, M.: The effect of acid–base clustering and ions on the growth of atmospheric nano-particles, Nat. Commun., 7, 11594, doi:10.1038/ncomms11594, 2016.

Li, C. and McMurry, P. H.: Errors in nanoparticle growth rates inferred from measurements in chemically reacting aerosol systems, Atmos. Chem. Phys., 18, 8979–8993, doi:10.5194/acp-18-8979-2018, 2018.

Mann, G. W., Carslaw, K. S., Spracklen, D. V., Ridley, D. A., Manktelow, P. T., Chipperfield, M. P., Pickering, S. J. and Johnson, C. E.: Description and evaluation of GLOMAP-mode: A modal global aerosol microphysics model for the UKCA composition-climate model, Geosci. Model Dev., 3(2), 519–551, doi:10.5194/gmd-3-519-2010, 2010.

McMurry, P. H.: Photochemical aerosol formation from SO2: A theoretical analysis of smog chamber data, J. Colloid Interf. Sci., 78(2), 513–527, doi:10.1016/0021-9797(80)90589-5, 1980.

Mulcahy, J. P., Jones, C., Sellar, A., Johnson, B., Boutle, I. A., Jones, A., Andrews, T., Rumbold, S. T., Mollard, J., Bellouin, N., Johnson, C. E. and Williams, K. D.: Improved Aerosol Processes and Effective Radiative Forcing in HadGEM3 and UKESM1, J. Adv. Model Earth Sy., 10, 2786–2805, doi:10.1029/2018MS001464, 2018.

Myhre, C. E. L., Nielsen, C. J. and Saastad, O. W.: Density and Surface Tension of Aqueous H2SO4 at Low Temperature, J. Chem. Eng. Data, 43(4), 617–622, doi:10.1021/je980013g, 1998.

Nieminen, T., Lehtinen, K. E. J. and Kulmala, M.: Sub-10 nm particle growth by vapor condensation – effects of vapor molecule size and particle thermal speed, Atmos. Chem. Phys., 10(20), 9773–9779, doi:10.5194/acp-10-9773-2010, 2010.

Pfeifer, J., Simon, M., Heinritzi, M., Piel, F., Weitz, L., Wang, D., Granzin, M., Müller, T., Bräkling, S., Kirkby, J., Curtius, J. and Kürten, A.: Measurement of ammonia, amines and iodine species using protonated water cluster chemical ionization mass spectrometry, Atmos. Meas. Tech. Discuss., 2019, 1–36, doi:10.5194/amt-2019-215, 2019.

Pichelstorfer, L., Stolzenburg, D., Ortega, J., Karl, T., Kokkola, H., Laakso, A., Lehtinen, K. E. J., Smith, J. N., McMurry, P. H. and Winkler, P. M.: Resolving nanoparticle growth mechanisms from size- and time-dependent growth rate analysis, Atmos. Chem. Phys., 18(2), 1307–1323, doi:10.5194/acp-18-1307-2018, 2018.

Stolzenburg, D., Steiner, G. and Winkler, P. M.: A DMA-train for precision measurement of sub-10 nm aerosol dynamics, Atmos. Meas. Tech., 10(4), 1639–1651, doi:10.5194/amt-10-1639-2017, 2017.

Stolzenburg, D., Fischer, L., Vogel, A. L., Heinritzi, M., Schervish, M., Simon, M., Wagner, A. C., Dada, L., Ahonen, L. R.,

Amorim, A., Baccarini, A., Bauer, P. S., Baumgartner, B., Bergen, A., Bianchi, F., Breitenlechner, M., Brilke, S., Buenrostro Mazon, S., Chen, D., Dias, A., Draper, D. C., Duplissy, J., El Haddad, I., Finkenzeller, H., Frege, C., Fuchs, C., Garmash, O., Gordon, H., He, X., Helm, J., Hofbauer, V., Hoyle, C. R., Kim, C., Kirkby, J., Kontkanen, J., Kürten, A., Lampilahti, J., Lawler, M., Lehtipalo, K., Leiminger, M., Mai, H., Mathot, S., Mentler, B., Molteni, U., Nie, W., Nieminen, T., Nowak, J. B., Ojdanic, A., Onnela, A., Passananti, M., Petäjä, T., Quéléver, L. L. J., Rissanen, M. P., Sarnela, N., Schallhart, S., Tauber, C., Tomé, A., Wagner, R., Wang, M., Weitz, L., Wimmer, D., Xiao, M., Yan, C., Ye, P., Zha, Q., Baltensperger, U., Curtius, J., Dommen, J., Flagan, R. C., Kulmala, M., Smith, J. N., Worsnop, D. R., Hansel, A., Donahue, N. M. and Winkler, P. M.: Rapid growth of organic aerosol nanoparticles over a wide tropospheric temperature range, P. Nat. Acad. Sci. USA, 115(37), 9122–9127, doi:10.1073/pnas.1807604115, 2018.

Figure S1: Typical experiment. Typical set of experiments at 5 °C and 60 % relative humidity. (a) shows the combined particle number size distribution measured with a DMA-train from 1.8-8 nm and above 8 nm with a TSI nano-SMPS. (b) shows the 50% appearance time of each channel measured at diameter d_{app} of the corresponding mobility sizer in the DMA-train (blue triangles), and the corresponding linear fits for both growing particle populations in two size intervals, 1.8-3.2 nm and 3.2-8.0 nm. (c) shows the simultaneously measured trace of sulfuric acid (red line) and ammonia (blue line). Sulfuric acid is produced by reaction with OH· radicals, which are formed by UV illumination of the chamber and the associated photo dissociation of ozone at constant ammonia level in the chamber. Different light intensities yield different levels of sulfuric acid, which in turn, yield different particle formation and growth rates. With increasing sulfuric acid concentrations not only the particle concentrations get higher but also growth gets faster. This is clearly visible by looking at the leading edge of the growing population, which can be identified due to short cleaning stages in between the experiments, where wall losses are increased due to increasing fan speed and lights are turned off. (d) shows the time series of the individual channels of the DMA-train at the fixed sizes (1.8-8 nm) during the same experiments (black solid lines), together with the sigmoidal shaped appearance time fits to the data, which determine the 50% appearance times shown in (b).
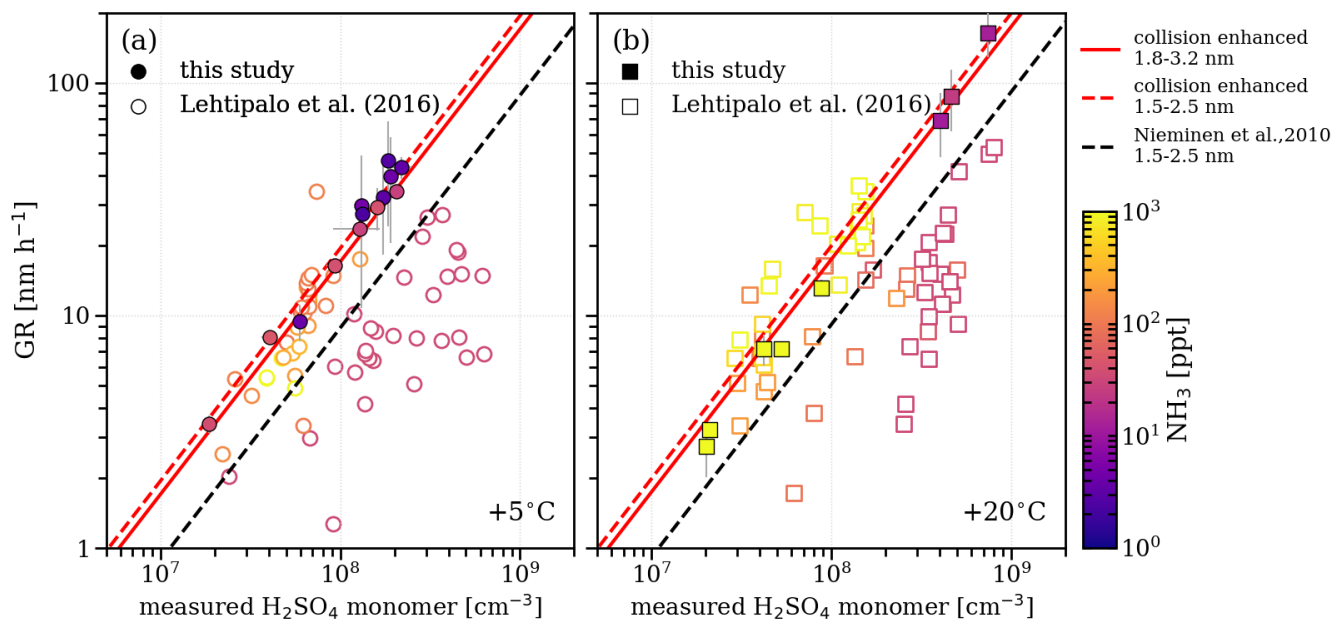
Figure S2: Comparison with a previous study. Comparison of the results from this study (filled symbols) with Lehtipalo et al. (2016) (open symbols) for two temperatures (a) 5 °C and (b) 20 °C. As the size range of the earlier study was smaller (1.5-2.5 nm), results with low NH_3 concentrations are considerably lower than the geometric limit of kinetic condensation (dashed black line) due to evaporation of sulfuric acid. As soon as ammonia is present in significant amounts, the earlier results agree well with the expected enhanced kinetic limit of condensation inferred in this study (dashed red line for 1.5-2.5 nm), also significantly above the geometric kinetic limit of condensation (Nieminen et al., 2010). The enhanced limit corresponding to the size range of the DMA-train measurements is also shown (red solid line 1.8-3.2 nm). Note that the ammonia measurements significantly improved between the two studies and that the lowest ammonia levels of the previous study are at the limit of detection of 35 ppt (green points) and the true value could be considerably lower.
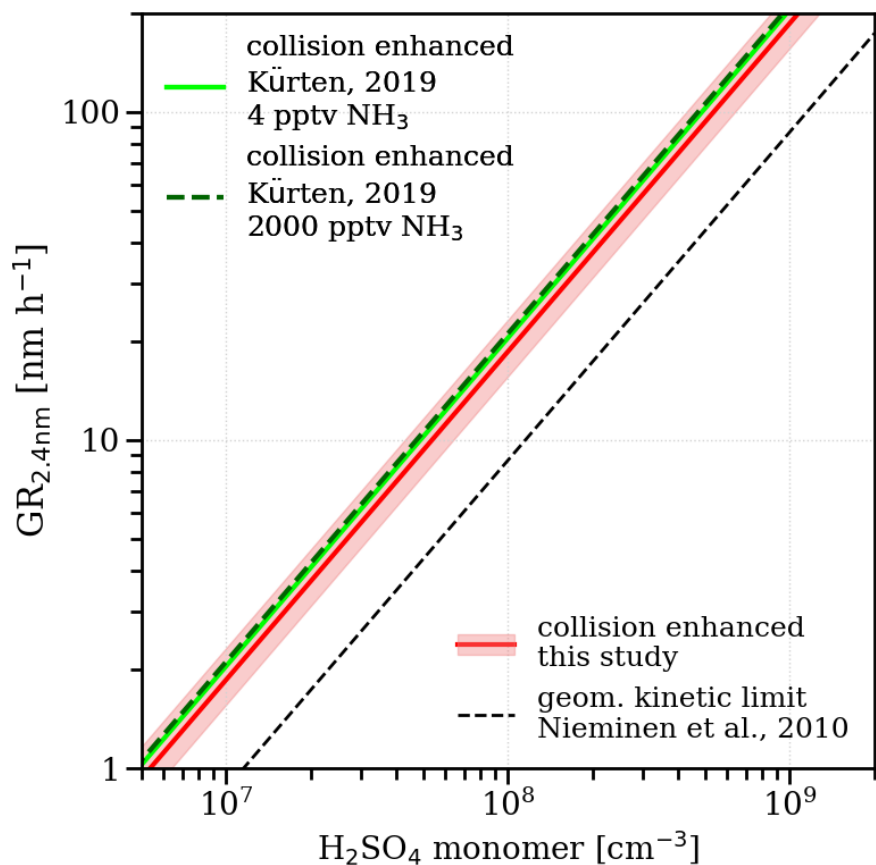
Figure S3: Modelling of the cluster contribution to growth. Comparison of the growth rate predictions at the kinetic limit of condensation for three different approaches at a diameter of 2.4 nm and 278.15 K versus sulfuric acid monomer concentration. The black dashed line shows the geometric limit of kinetic condensation (Nieminen et al., 2010), the red line and red area show the result of this study and its systematic uncertainty, and the light green line and the dark green dashed line show the predictions of a model which includes sulfuric acid/ammonia clustering and evaporation (Kürten, 2019), for 4 pptv and 2000 pptv ammonia (and assumed sulfuric acid density of $\rho=1.615$ g cm^{-3}), respectively. The additional clustering and therefore cluster contribution to growth at higher ammonia levels is insignificant in the model confirming that the effect of hidden sulfuric acid can be neglected for our set of experiments.
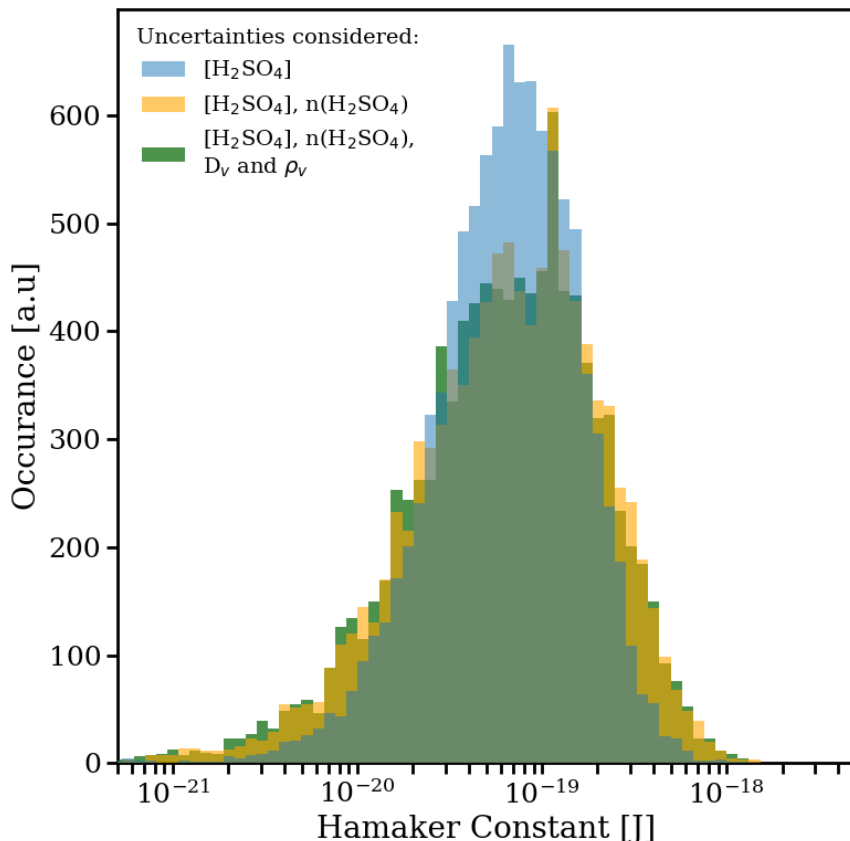
Figure S4: Systematic uncertainty estimate. Results from a Monte-Carlo estimate of the systematic uncertainty of our Hamaker constant measurement. Every histogram represents the outcome of 10000 Hamaker constant fits to our dataset with randomly assigned systematic parameters. For every colour other systematic uncertainties are additionally considered. The systematic uncertainty from the sulfuric acid measurement (the only considered uncertainty in the blue histogram) dominates the width of all the result distributions. While the water content of the condensing cluster (additionally considered in the yellow histogram) still broadens and skews the distribution slightly, the effects of different assumptions on the diffusion coefficient and density of sulfuric acid (additionally considered in the green histogram) are completely negligible. This uncertainty estimate yields the 68% confidence interval for the Hamaker constant of $[2.7 \cdot 10^{-20}, 1.5 \cdot 10^{-19}]$ J, however the excellent agreement of the median of our results $6.6 \cdot 10^{-20}$ J with previous measurements (Chan and Mozurkewich, 2001; McMurry, 1980) suggests that the systematic uncertainty of the sulfuric acid measurement could be much smaller than previously assumed.